

# Numerical Simulation of Rocket Engine Internal Flows

Project Representative

Nobuyuki Tsuboi JAXA's Engineering Digital Innovation Center, Japan Aerospace Exploration Agency

Authors

Taro Shimizu JAXA's Engineering Digital Innovation Center, Japan Aerospace Exploration Agency

Nobuhiro Yamanishi JAXA's Engineering Digital Innovation Center, Japan Aerospace Exploration Agency

Chisachi Kato Institute of Industrial Science, The University of Tokyo

Kaoru Iwamoto Department of Mechanical Systems Engineering, Tokyo University of Agriculture and Technology

At a start-up transient of the rocket engine, a large pressure disturbance, called ignition overpressure (IOP), is generated, which is one of the concerns on the modifications from the H-IIA to H-IIB. We estimate the side-load acting on the actuator of the nozzle by IOP. This is taken into consideration at the early development process of the H-IIB rocket. We have also carried out Large Eddy Simulation of cavitating flows in the inducers that are designed for the next-generation rocket engine turbopump. The computational mesh consists of approximately 20 million hexahedral elements, which is fine enough to evaluate the turbulent boundary layer on the inducer blades. Direct numerical simulation of a turbulent channel flow at  $Re_{\tau} = 2320$  was made in order to examine the mechanisms of the production and dissipation of the kinetic energy at high Reynolds numbers. Not only the near-wall streaky structures and vortices ( $y^+ \sim 15$ ), but also the hierarchical structures ( $150 \nu u_{\tau} < y < \delta$ ) actively produce the turbulent kinetic energy more than their own dissipation.

**Keywords:** H-IIB rocket, LE-7A, ignition overpressure, rocket turbopump, cavitation, large eddy simulation, direct numerical simulation, high Reynolds number, wall turbulence

## 1. Ignition overpressure

The H-IIB launch vehicle, which is an upgraded version of the current H-IIA launch capacity, is under development. The H-IIB launch vehicle has two major purposes. One is to launch the H-II Transfer Vehicle (HTV) to the International Space Station (ISS). The other is to respond to broader launch needs by making combined use of both H-IIA and H-IIB launch vehicles. To obtain larger launch capability, the H-IIB has two (clustering) liquid rocket engines (LE-7A) in the first-stage, instead of one for the H-IIA. Therefore, the estimation of the difference of flow fields between single and clustering nozzle configurations is important.

In this study, the generation of the large pressure disturbance at the start-up transient, called ignition overpressure (IOP) is numerically investigated in detail, which is one of the concerns on the modifications. A three-dimensional compressible Navier-Stokes solver is used to capture the unsteady flow structure<sup>1-2)</sup>. This solver has good results for the other study on a combustion flow inside the rocket nozzle<sup>3)</sup>. Under the single nozzle configuration (not shown here), the result shows that at the start-up transient, an overpressure and a vortex ring are generated and propagate downstream from the nozzle. The nozzle tip pressure is compared between the numerical simulation and the experiment. The agreement is fairly good. Under the clustering nozzle configuration, the

interaction between the overpressure waves and the vortex rings may occur especially between the nozzles.

Figure 1 shows the numerical result of the simultaneous start-up. The left column represents Mach number and the right column represents pressure field. As the ratio of the chamber pressure to the ambient (NPR) increases, the separation shock wave is formed inside the nozzle and the overpressure propagates outside the nozzle spherically. When  $NPR=8.9$  (Fig. 1 c)), the interaction of the overpressure stands out and generates the positive pressure disturbances on the nozzle wall, which generates repulsive force between nozzles. Then it is found that the interaction of two vortex ring (shown as four blue circles in pressure field) occurs, which induces the anomalous behavior that the inner part of the interacting vortex ring propagates upstream (Fig. 1 e)). This generates negative pressure disturbances and asymmetric wall pressure distribution on each nozzle. Thus, the force acting on the nozzle becomes again asymmetric. We estimate the side-load acting on the actuator of the nozzle by the simulation, which is taken into consideration at the early development process before the firing test.

## 2. Turbomachinery simulation

To achieve stable operations at a high rotational speed under a low inlet pressure, rocket engine turbopumps are

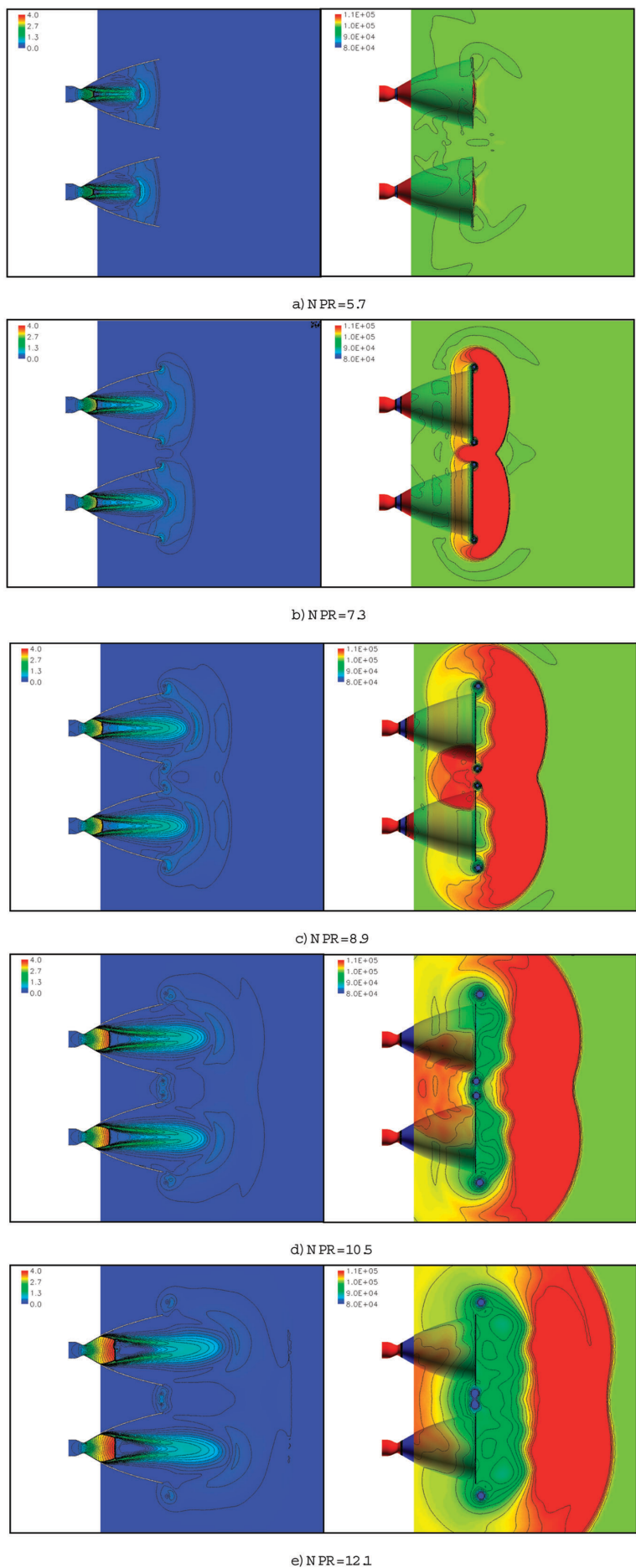


Fig. 1 Mach number distribution (left column) and pressure field (Pascal; right column).

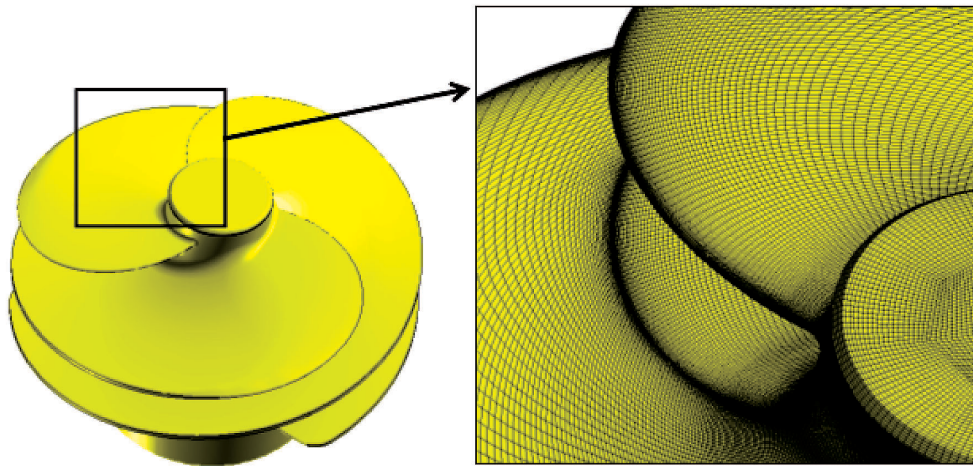


Fig. 2 Inducer geometry and computational mesh.

generally equipped with an axial-flow inducer stage. As the inlet pressure is decreased and local pressure becomes lower than the vapor pressure, cavitation gradually develops on the suction side of inducer's blades and/or near their tip and finally leads to the breakdown of the inducer performance. In addition, cavitation instabilities, such as rotating cavitation and cavitation surge, are often observed in experiments and they cause serious shaft vibration and/or fluctuations of the blade stresses. Therefore, it is an important issue to understand the physical mechanism of unsteady cavitation phenomena related to internal flows of a turbopump inducer.

Computational Fluid Dynamics (CFD) is becoming an important tool for designing and developing reliable turbomachinery. For evaluating the static characteristic of cavitation, computations with Reynolds Averaged Navier-Stokes Simulation (RANS) are often used and some reliable results are obtained. However, we cannot accurately predict cavitation-related unsteady phenomena with RANS since RANS is essentially based on the time-averaging concept and models dynamics of all turbulent effects. On the other hand, a large eddy simulation (LES) directly deals with dynamics of the eddies resolved with the computational grids, and it is suitable for computing unsteady flows related cavitation.

In the previous fiscal year, we developed an LES code for accurate computations of unsteady flows in turbomachinery, and performed computations of cavitating flows for a test inducer. In this fiscal year, we have carried out LES analyses of cavitating flows in the inducers that are designed for the next-generation rocket engine turbopump.

In LES calculations, we often need to evaluate small but active eddies in the turbulent boundary layer accurately since they essentially determine the characteristics of the flow. Therefore, it is very important to use highly accurate and stable numerical method and sub-grid scale (SGS) model. Our LES code solves the Navier-Stokes equations of incompressible flow, in which dynamic Smagorinsky model

is implemented as SGS model. The code is based on a finite element method with hexahedral elements and has the second-order accuracy both in time and space<sup>4</sup>). By the multi-frame of reference function based on an overset method, it is possible to compute rotor-stator interactions<sup>5</sup>). For computation of cavitating flows, we have implemented the cavitation model proposed by Okita et al.<sup>6</sup>) In this model, the evolution of cavitation is represented by source/sink of the vapor phase in incompressible liquid flows, and compressibility is taken into account through the low Mach number assumption.

The inducer in this study has three helical blades with swept-back leading edge. The calculations were performed at the designed operation point. Computational mesh on the inducer's blades is shown in Fig. 2. The total mesh consists of approximately 20 million hexahedral elements. The clearance flow between the blade tip and casing inner wall is resolved with more than fifteen layers of grid. In Fig. 3, vortical structures on the surface of inducer blades is visualized by showing instantaneous iso-surfaces for  $\Delta p = 200$ . Streaky

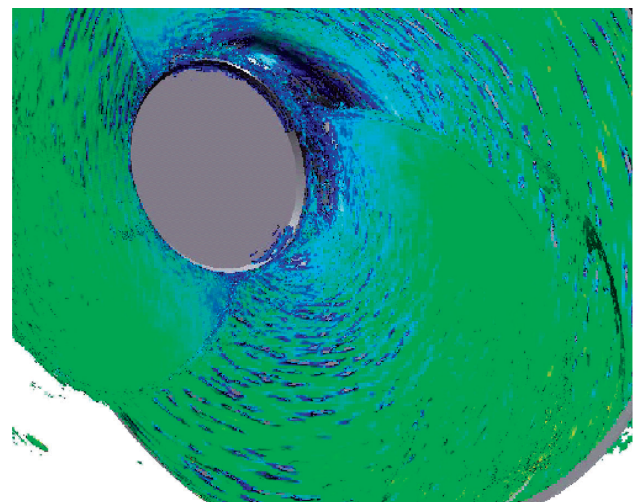


Fig. 3 Instantaneous vortical structure on the surface of blades (Iso-surfaces with  $\Delta p = 200$  : color represents static pressure).

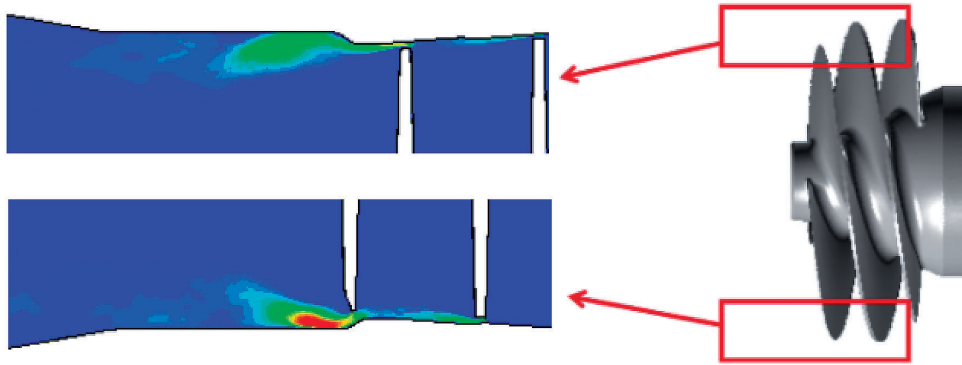


Fig. 4 Time-averaged axial velocity distribution (bright colors represent backflow component).

structures are clearly seen, which confirms that resolution of the present computational mesh is fine enough to evaluate the turbulent boundary layer at least qualitatively. It is known that the leakage flow through the tip clearance is generally formed in inducers. Figure 4 shows the axial velocity distribution near the tip. Contours with bright colors represent the backflow region. Note that the leakage flow goes towards the upstream direction. The axial length of this leakage flow region is almost independent whether the flow is non-cavitating or cavitating as long as the cavitation number  $\sigma$ , is above 0.18. In the shear layer between the leakage flow (i.e., backflow) and the main flow, intense vortices are formed as shown in Fig. 5. Figure 6 shows instantaneous cavity structures for different cavitation numbers,  $\sigma = 0.20$  and 0.18. In  $\sigma = 0.20$ , cavitation takes place only along the

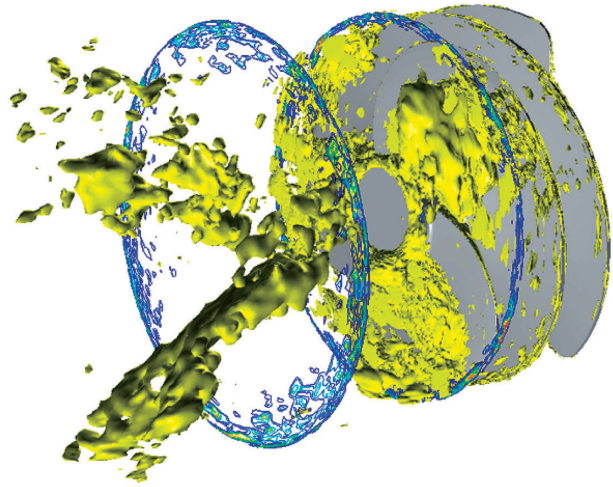


Fig. 5 Backflow vortices and axial velocity distribution.

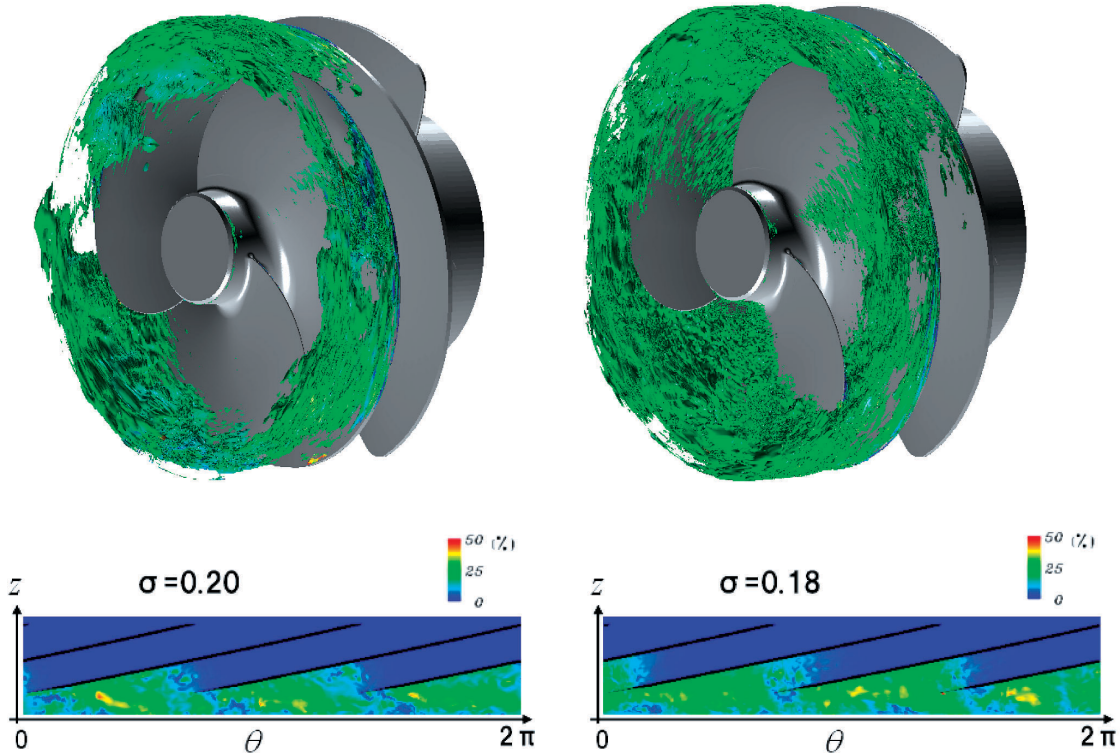


Fig. 6 Cavity structures visualized by iso-surfaces with void ratio of 0.15 (upper figures) and contours of void ratio (lower figures) for  $\sigma = 0.20$  (left) and 0.18 (right).

tip leakage flow. As the cavitation number,  $\sigma$  becomes smaller, the cavitation is generated in a broader region, not only near the casing wall but also on the blade surface and in the blade passages. The cavitation predicted in this result is almost symmetric and the cavity rotates with the same rotational speed as the inducer blades. In the lower panels in Fig. 6, the contour of void ratio in the cascade is shown on the  $\theta$  (circumferential direction) –  $z$  (axial direction) plane. The inlet flow is in the positive direction. For  $\sigma = 0.20$ , the cavitation tends to grow with the tip leakage flow and the cavity structure extends towards the upstream of the inducer. On the other hand, for  $\sigma = 0.18$  the cavity develops on the blade surface and fills in the blade passages. Therefore, the characteristic of the cavity structures changes as the cavitation number decreases from  $\sigma = 0.20$  to  $\sigma = 0.18$ . Figure 7 indicates the frequency spectra of the pressure fluctuations on the casing wall, where comparisons are made between cavitating from  $\sigma = 0.20$  to  $\sigma = 0.18$  cases and non-cavitating case. Several peaks appear in the spectra for both cases. The component with large amplitude at a frequency of  $3\omega$  corresponds to the blade passing frequency (BPF) and its amplitude does not depend whether the flow is cavitating or non-cavitating. It is known that if a cavitating flow is unstable due to rotating cavitation or cavitation surge, a peak appears near the shaft rotational frequency  $\omega$  in the upstream of the inducer. In this calculation, there is no peak near  $\omega$ . Therefore, it is concluded that no unstable cavitating mode grows in  $\sigma = 0.18$  and  $0.20$  cases.

### 3. Channel flow simulation

Some fundamental characteristics of a turbulent channel flow at  $Re_\tau = 2320$  are studied by means of direct numerical simulation (DNS). Our aim is to accumulate the essential knowledge on high-Reynolds number wall-turbulence, which can be used for improvement of turbulence models, such as subgrid-scale model in above-mentioned LES.

The numerical method used in the present study is a pseudo-spectral method. See Ref. [7] for the numerical procedures and parameters in detail. Hereafter,  $u$ ,  $v$ , and  $w$  denote the velocity components in the streamwise ( $x$ -), wall-normal ( $y$ -), and spanwise ( $z$ -) directions, respectively. Superscript (\*) represents quantities non-dimensionalized with the friction velocity  $u_\tau$  and the kinematic viscosity  $\nu$ .

Figure 8 shows the ( $y$  -  $z$ ) cross-stream plane of an instantaneous flow field, in which contours of production, dissipation and production minus dissipation terms of turbulent kinetic energy are visualized. It is found that away from the wall, the turbulent kinetic energy is produced mainly in the large-scale low-speed structures and partly in the large-scale high-speed ones. Namely the large-scale structures have the large effect upon the production of the kinetic energy. On the other hand, the profile of the dissipation is correspond to the small-scale structures mainly in the large-scale low-speed structures. It is also found through Fig. 8(c) that not only the near-wall streaky structures and vortices ( $y^+ \sim 15$ ), but also the hierarchical structures in the low-speed large-scale motions ( $150 \nu/u_\tau < y < \delta$ , where  $\delta$  is the channel half width) actively produce the turbulent kinetic energy more than their own dissipation.

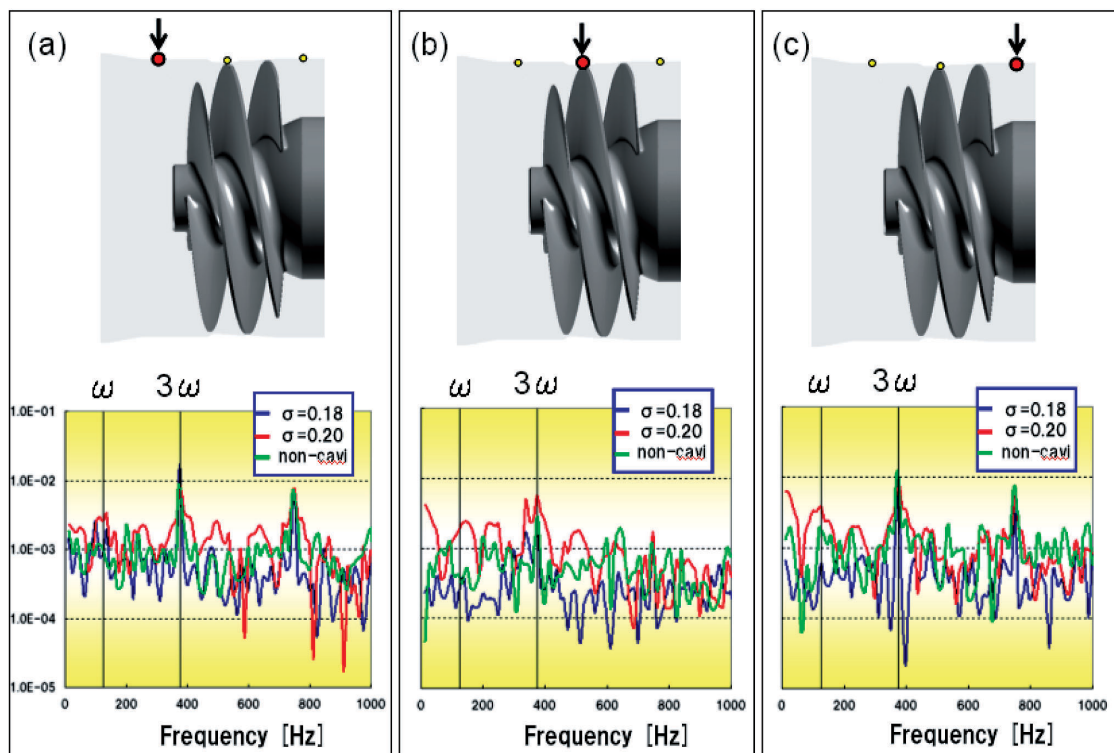


Fig. 7 Frequency spectra of pressure fluctuations on the casing wall for (a) upstream, (b) middle, and (c) downstream of the inducer blade.

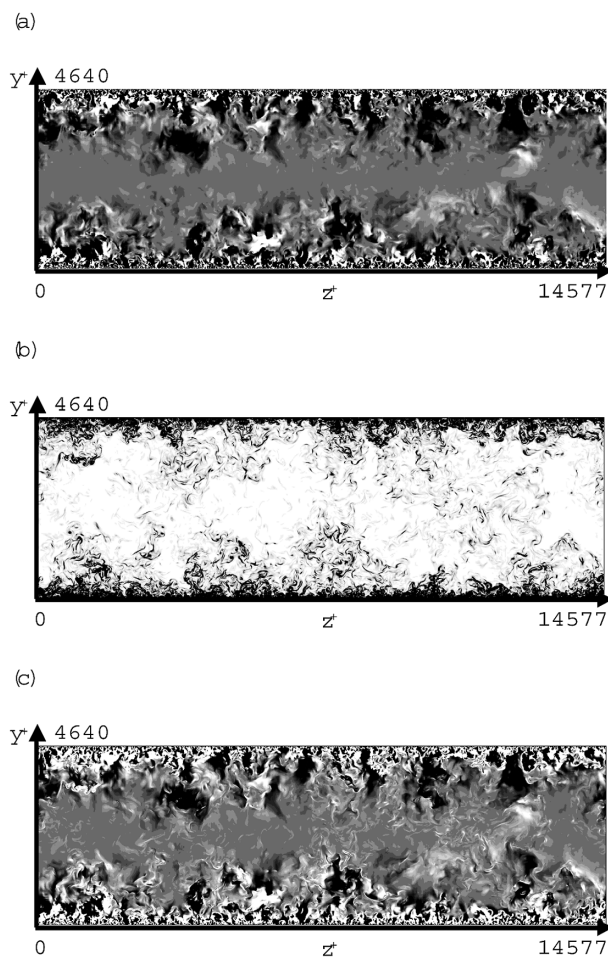


Fig. 8 Cross views of (a) production (b) dissipation (c) production minus dissipation terms of turbulent kinetic energy for the instantaneous velocity field. (a), (c) white to black, negative to positive; (b) white to black, zero to positive.

### References

- [1] Kodera, M., Sunami, T., Nakahashi, K., "Numerical Analysis of SCRAMJET Combusting Flows by Unstructured Hybrid Grid Method," AIAA Paper, 00-0886, Jan. 2000.
- [2] Tohoku University Aerodynamic Simulation Code (TAS).
- [3] Shimizu, T., Miyajima, H., and Kodera, M., "Numerical Study of Restricted Shock Separation in a Compressed Truncated Perfect Nozzle," AIAA Journal, Vol.44, No.3, pp.576-584, 2006.
- [4] C. Kato, and M. Ikegawa, "Large Eddy Simulation of Unsteady Turbulent Wake of a Circular Cylinder Using the Finite Element Method," ASME-FED, 117, 49-56, 1991.
- [5] C. Kato, M. Kaiho, and A. Manabe, "An Overset Finite-Element Large-Eddy Simulation Method with Application to Turbomachinery and Aeroacoustics," Trans. ASME, 70, 32-43 (2003).
- [6] K. Okita, thesis of Osaka University (in Japanese), 2002.
- [7] K. Iwamoto, N. Kasagi, and Y. Suzuki, "Direct numerical simulation of turbulent channel flow at  $Re_\tau = 2320$ ," Proc. 6th Symp. Smart Control of Turbulence, pp.327-333, Tokyo, Japan, Mar. 2005.

## ロケットエンジン内部流れのシミュレーション

プロジェクト責任者

坪井 伸幸 宇宙航空研究開発機構 情報・計算工学センター

著者

清水 太郎 宇宙航空研究開発機構 情報・計算工学センター

山西 伸宏 宇宙航空研究開発機構 情報・計算工学センター

加藤 千幸 東京大学 生産技術研究所

岩本 薫 東京農工大学大学院 工学府機械システム工学

国産ロケットの信頼性向上及び将来型宇宙輸送システムの開発に資するため、主要エンジン要素(燃焼器系・供給器系)で発生している諸問題を再現できるCFDコードを開発し、概念設計・システム評価・不具合対策等に使用し、試作・試験のサイクルを短くすることを目標に、プロジェクトを進めている。本年度は、以下の3つのテーマについて解析を実施した。

次期H-IIBロケットで採用されるクラスタノズル(液体ロケットが2基)の設計開発に資するため、特に起動時の過大圧力波動の発生について詳しく調べた。計算結果から、圧力波動と渦輪の干渉が捉えられ、それにより発生する横力等が定量的に評価できた。得られた結果は今後の詳細設計に反映される。

H-IIBロケットの開発に資するため、LE-7Aエンジン液体酸素ターボポンプの入口に装備される改良設計インデューサのキャビテーション非定常特性を評価した。候補として挙げられた4種類のインデューサ形状についての大規模非定常LES解析を実施し、それぞれのインデューサ内部流れにおける逆流構造、翼面上の圧力分布等を水流し試験結果と比べた結果、良い一致を示した。また、キャビテーションによって不安定事象が発生しないことを事前に確認することができた。本シミュレーションによって評価されたインデューサは液体酸素ターボポンプ試験に供することが決まっており、H-IIBロケットの開発に大きく貢献することができた。

高レイノルズ数壁乱流で用いることのできる高精度乱流粗視化モデルの構築を目的として、世界最大のレイノルズ数( $Re_\tau = 2320$ )平行平板間乱流直接数値シミュレーション(DNS)を行い、乱れエネルギーの生成・散逸量をデータベースより求めた。低レイノルズ数では、乱れエネルギーは緩和層のみにおいて超過生成される。他方、高レイノルズ数では、対数領域の一部(大規模低速領域内の階層構造)においても超過生成されることがDNSを用いて初めて分かった。

キーワード: H-IIB ロケット, LE-7A エンジン, 過大圧力変動, ターボポンプ, LES, 高レイノルズ数壁乱流, DNS